

Dynamical downscaling with COSMO and COSMO-CLM in the Sino-Mongolian Altai region

Frederik Kurzrock¹ · Andreas Buerkert⁴ · Oyunmunkh Byambaa² · Sven Goenster⁴ · Luxi Jin² · Christian Ohlwein² · Clemens Simmer²  · Thorsten Simon³

Received: 16 April 2016 / Accepted: 4 November 2016 / Published online: 19 November 2016
© The Author(s) 2016. This article is published with open access at Springerlink.com

Abstract For the first time, regional atmospheric simulations with spatial resolution down to 6 km have been performed in the Sino-Mongolian Altai region using the COSMO weather forecast and regional climate model. Two 5-year periods (1979–1982 and 2008–2012) have been simulated for a first evaluation of the model in this special region. The added value of a dynamical downscaling with the COSMO regional climate model CCLM towards the driving ERA-Interim reanalysis is investigated by comparison with weather station observations. In the mountainous region, the CCLM simulation much better relates to the observed monthly mean 2 m temperature and maximum monthly precipitation sums in summer than ERA-Interim. In addition, the intensity distribution of sub-daily precipitation amounts becomes more realistic with increasing altitude. CCLM does, however, overestimate convection in the mountains and accordingly simulates too much precipitation. Moreover, wintertime near-surface temperature inversions are underrated in the southern near-Gobi area, which leads to too high 2 m temperatures in that region. To examine the ability of the COSMO model to reproduce the vertical thermodynamic structure of the

troposphere, additional simulations with the weather forecast version of COSMO were performed for July 2013 and compared to radiosonde measurements of the WATER-COPE field experiment in this region. The results indicate that the COSMO model is quite capable of qualitatively simulating a range of features of the local tropospheric stratification. Mean differences between observed and simulated dew point and temperature profiles were in the range of only to 1–2 °C in the lower troposphere.

1 Introduction

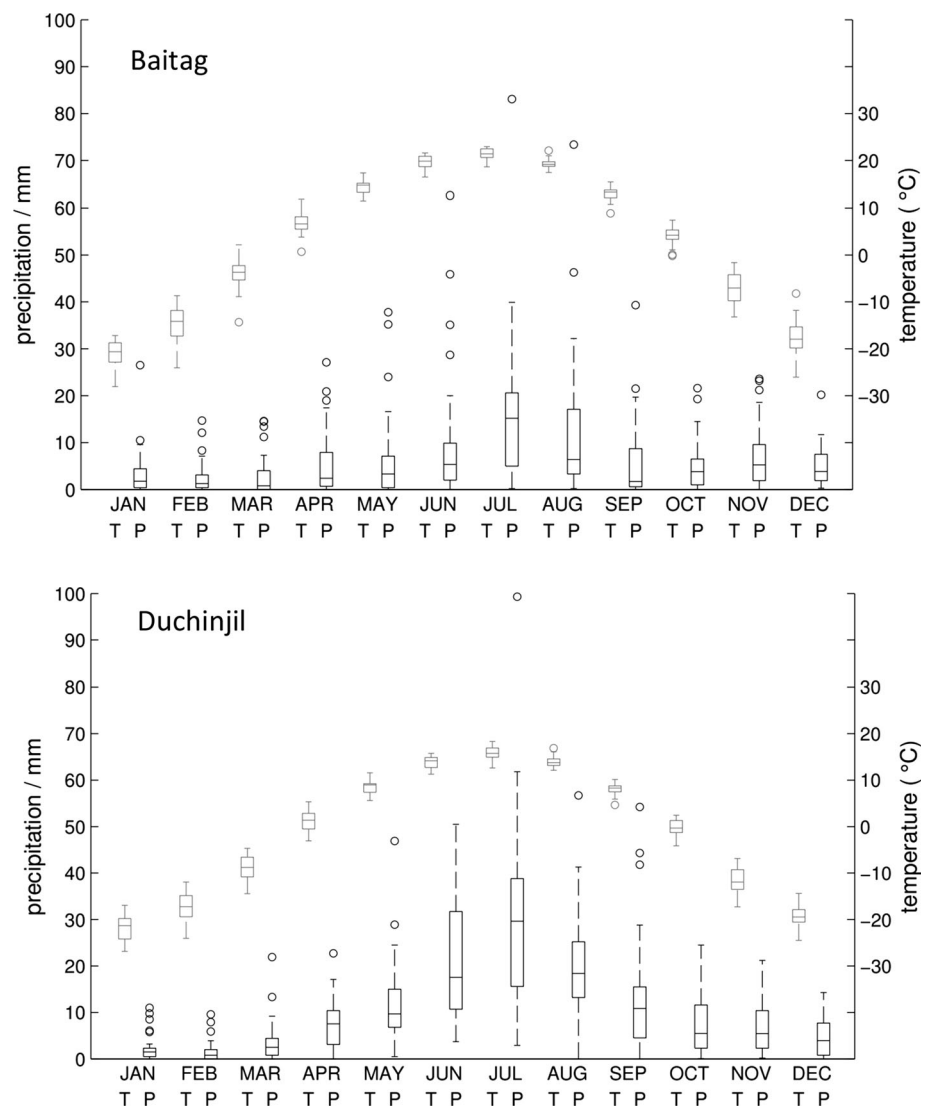
The Sino-Mongolian Altai region in Central Asia, where western Mongolia borders China, is characterized by highly continental climatic conditions resulting in high intra-annual and diurnal temperature variations. The summer is rather short and hot; the major atmospheric circulation systems influencing Central and South-Eastern Asia barely touch and never dominate the region (Pederson et al. 2000). Winter is often dominated by long-lasting low temperatures, clear skies, and extremely low precipitation due to the Siberian anticyclone. Accordingly, monthly precipitation sums rarely exceed 10 mm in winter, as demonstrated by observations of two climate stations for the time period between 1979 and 2012, as shown in Fig. 1. The largest monthly precipitation amounts occur during summer with a peak in July reaching up to 60 mm. Precipitation sums are larger at elevated locations due to the orographic influence on convection. As the Sino-Mongolian Altai extends roughly from North to South, it represents an orographic barrier for westerlies. Air masses crossing the Altai are transformed in different ways, which lead to a large variety in the mesoclimate and regional

Responsible Editor: A. P. Dimri.

✉ Clemens Simmer
csimmer@uni-bonn.de

- ¹ ESPACE-DEV, Université de La Réunion, Réunion, France
- ² Meteorological Institute, University of Bonn, Bonn, Germany
- ³ Institute of Atmospheric and Cryospheric Sciences, University of Innsbruck, Innsbruck, Austria
- ⁴ Faculty of Organic Agricultural Science, University of Kassel, Kassel, Germany

Fig. 1 Box-whisker diagrams of monthly precipitation sums (black symbols left scales) and monthly mean 2 m temperatures (grey symbols right scales) for the weather stations Baitag (upper panel) and Duchinjil (lower panel) during the time period 1979–2012. The station locations are indicated by stars in Fig. 2. The lower and upper bounds of the boxes represent the 25th and 75th percentiles, respectively. The whiskers encompass the most extreme data points, which are not considered as outliers shown as circles. Information on the utilised data and the stations locations is given in Sect. 3.1



circulation processes (Batima 2006; Bezuglova et al. 2012).

The accurate simulation especially of winter temperatures is crucial for impact studies concerning the Mongolian herding economy. Some winters, e.g., the winter 2010/11, were exceptionally cold and constituted extremely harsh conditions for herders. Winters in which herders lose large amounts of their livestock, the so-called 'zuds', are mostly accompanied by exceptionally cold temperatures and can have severe consequences, since herding is still a major component of the Mongolian society and economy (Siurua and Swift 2002). Thus, there is a need especially for projecting the future occurrence of zuds (Batima et al. 2008).

During the last 60 years, over Mongolia, annual near-surface air temperature has increased by 1.9 °C with stronger warming in winter (by 3.6 °C) and only a slight increase in summer by 0.5 °C (Batima et al. 2005;

Gomboluudev 2012). The number of hot days increased by 16–25 days and cold days decreased by 13–14 days in the period between 1961 and 2007 (Dagvadorj et al. 2010). Annual mean precipitation slightly decreased for the period between 1940 and 2001 (Batima et al. 2005). A stronger warming (Yatagai and Yasunari 1994; Yin 2006) and a slight increase of precipitation have been observed in the Altai region compared to other regions of Mongolia (Batima et al. 2005; Dagvadorj et al. 2010; Gomboluudev 2012).

Concerning atmospheric sciences, the interest in the rather remote Altai region, especially the Sino-Mongolian part, has been relatively low, but some climate-related research has been conducted recently. Because of the sparse meteorological records in the region, climatic proxies, including lake sediment, tree rings, and ice cores, are used to reconstruct the spatial and temporal climate variability and changes in this region (Davi et al. 2015;

Dulamsuren et al. 2014; Schluetz and Lehmkühl 2007; Schwikowski et al. 2009) and its impact on glaciers (Kamp et al. 2013) and forests. Most tree ring-based past climate reconstruction studies in Western Mongolia (Davi et al. 2015; Davi et al. 2009) and north-western China (Chen et al. 2012, 2014; Zhang et al. 2015) identified a significant climate and environmental change with rapid warming and precipitation increases caused by a general intensification of the global hydrological cycle. Bezuglova et al. (2012) analysed the thermal regime of the Russian and northern part of the Mongolian Altai for the period between 1940 and 2008 using averaged monthly temperature observations. During the considered time period, a temperature increase was registered, which was most significant during the cold seasons.

There is an increasing demand of decision makers for high-resolution information, e.g., on water resources, for the past and the future with regard to global warming to avert socio-economic damage and develop adaptation strategies (Dairaku et al. 2008; Fowler et al. 2007; Leung et al. 2003; Viviroli et al. 2011). Due to the coarse resolution, global reanalysis data sets, such as ERA-Interim (Dee et al. 2011), usually cannot resolve complex orography and spatially variable regional climates. As applications, such as hydrological or ecological modelling, call for high-resolution climate data, a downscaling of global climate model (GCM) or reanalysis data is thus inevitable (Bastola and Misra 2014; Flint and Flint 2012). Various downscaling methods have been assessed, e.g., by Fowler et al. (2007) with respect to hydrological modelling. Their results suggest little advantages of dynamical downscaling over statistical methods at least for the present day climates. In the recent decades, however, dynamical downscaling has improved and become a common technique for adding information on regional scales to global simulations (Giorgi et al. 2001; Rummukainen 2010). Many studies examined the additional variability of regional climate models (RCMs) which constitute an 'added value' to the variability of their driving GCMs. Simon et al. (2014) presented a new method for determining the temporal scales on which added value can be found in an RCM; they proved that internal variability is generated by the RCM with much higher frequencies than by the driving GCM.

Several studies utilizing RCMs demonstrate the merits of dynamical downscaling in Asia for hindcasts and future projections (Chotamonsak et al. 2011; Kim et al. 2008; Ozturk et al. 2012; Qian et al. 2003; Sato and Xue 2013; Schiemann et al. 2008). However, it has to be kept in mind that inter-model variations can be substantial (Fu et al. 2005; Leung et al. 1999). The RCM COSMO-CLM (CCLM; Rockel et al. 2008) has been applied and evaluated over Asia, e.g., by Dobler and Ahrens (2008, 2010)

and Rockel and Geyer (2008). Wang et al. (2013) investigated the performance of CCLM for the East Asia domain defined by CORDEX (Coordinated Regional Climate Downscaling Experiment, Giorgi et al. 2009). They found that the CCLM has the potential to improve the global fields of driving models and resolve important small-scale features of East Asia monsoon dynamics. However, their ERA-40 driven simulations show a pronounced wet bias in the north of the domain, which covers also the Sino-Mongolian Altai.

Several downscaling studies for Central Asia do exist with horizontal grid spacing down to 20–30 km using different models (Gao et al. 2011; Kim et al. 2008; Klehmet et al. 2013; Liu et al. 2013; Mannig et al. 2013; Maussion et al. 2014; Sato et al. 2007). These studies focus on future projections and/or the better representation of Asian monsoon dynamics in the RCM simulations. The quality of the simulations depends on the type of model and its parameterisations, the simulated year, or season (dry/wet) as well as the orography and lateral boundary conditions. The model domains in these studies contain either the Altai Mountains or regions adjacent to it. Sato et al. (2007) applied the RCM TERC-RAMS in Mongolia for the 1990s with a grid spacing of 30 km and found that the rainfall distribution was generally simulated well, whereas precipitation was overestimated in the Altai. The model domain of Klehmet et al. (2013), who applied CCLM in Siberia with a grid spacing of 0.44° , also contains the Altai region in the southwest. In their study, CCLM is able to add spatial detail in terms of snow water equivalent (SWE), especially at mountain ranges, while there is a tendency to overestimate SWE in mountainous terrain. Concluding, they find that CCLM provides a clear added value compared to reanalyses, considering SWE.

To this day, there is no dynamical downscaling study in the referred literature, which focuses on the Altai region, and there are no published results of atmospheric simulations with horizontal resolutions higher than 30 km for the Sino-Mongolian Altai. There does exist, however, a report on a 10 km resolution downscaling for the period 2000–2010 and a projection for the years 2011–2030 for hydrological impact studies published by the World Wildlife Funds (WWF, 2012).

In our study, we investigate the performance of a state-of-the-art high-resolution limited-area model with an even higher grid spacing of 0.0625° (approximately 7 km) over the Sino-Mongolian Altai region. We focus in particular on the potential of dynamical downscaling and regional climate modelling in the Altai region using the limited-area model COSMO (Consortium for Small-Scale Modelling; <http://www.cosmo-model.org>). We are aware of statistical downscaling techniques as an alternative (see, e.g., discussions in Murphy 1999 and Wood et al. 2004), but

evaluated only dynamical downscaling, since hydrological predictions, which need distributed forcing fields, will be the main application.

As the observational network is coarse and the terrain of the study region is complex, a detailed model validation is hardly possible. This study aims at evaluating the model performance using a small number of climate stations, and in addition, radio soundings performed during an experiment. We address the question whether the key parameters 2-m temperature and surface precipitation are spatially and temporally represented better in the COSMO simulations, than in the driving global reanalysis data set ERA-Interim. The capability of COSMO to represent the vertical structure of the atmosphere in this region in terms of temperature and humidity is evaluated using radio soundings conducted during a field campaign in July 2013.

The outline of this paper is as follows. In Sect. 2, the model setup and an overview of the performed simulations are presented. The observational data used for the evaluation of the simulations are described in Sect. 3. Section 4 first compares ERA-Interim with CCLM downscaling results for two 5-year periods (1979–1982 and 2008–2012) for the summer and winter seasons, followed by a detailed comparison of ERA-Interim and its downscaling with climate station observations and a simulation of the weather forecast version of COSMO with radiosonde observations. The results are discussed in Sect. 5, and a summary and conclusions are provided in Sect. 6.

2 Model description and setup

We evaluate simulations carried out with both the climate version and the weather forecast version of the COSMO model, which is operationally used by the German and other Meteorological Services. COSMO is a three-dimensional, fully compressible, and non-hydrostatic limited-area model. The prognostic thermo-hydrodynamic equations for compressible flow in a moist atmosphere are solved on an Arakawa-C grid (Arakawa and Lamb 1977) in a geographical coordinate system with a rotated pole for allowing close to equal-area grid cells over the particular regions of interest. In the vertical, a hybrid terrain following height coordinate with variable discretization is used. A detailed description of model dynamics, numerical schemes, and physical parameterisations can be found in Doms (2011) and Doms et al. (2011), and Bachner et al. (2008) made an extensive evaluation of the different sets of physical parameterizations on the simulation of precipitation. The main differences between the forecast and climate versions of the COSMO model mainly relate to technical features required for climate runs. Thus, the use of dynamic boundary data, varying CO₂ concentrations,

and a scale-selective type of relaxation (spectral nudging) are additionally possible in CCLM. Furthermore, CCLM includes modifications of its land model TERRA, the possibility to use restart files and additional output variables (Boehm et al. 2006).

For the regional climate simulations version, COSMO4.8-CLM11 was used, which is maintained and provided by the Climate Limited-Area Modelling-Community (CLM Community; <http://www.clm-community.eu>). The weather simulations have been performed with version 4.21 of the COSMO model. In the following, the regional climate simulations are referred to as CCLM simulations, while the term COSMO is used for the weather forecast model simulations. Figure 2 shows the model domain and the orography on a latitude–longitude grid centred in north-western China. The grid comprises 200 × 170 grid boxes with a rotated north pole at 43.56°N/90.95°W. A grid spacing of 0.0625° (ca. 7 km) and 40 vertical layers were used. The domain spans the region from Tian Shan and eastern Kazakhstan in the west to Gobi-Altai and the Khangai Mountains in the east. It covers the Chinese and Mongolian Altai and most of the Russian Altai. As most of the moisture is transported to the region with prevailing westerly winds in summer, the domain is enlarged in the west to minimise unwanted boundary-zone effects in the inflow region. Effects of the Tian Shan Mountains in the south-western boundary region of the domain on the simulation results in the study region are also minimised this way. The orography used in the CCLM and COSMO simulations is not exactly the same; the surface altitudes of the grid columns slightly deviate from each other, since the model runs were performed on different machines and with different versions of the model system. These differences are, however, not significant for the analyses performed in this study.

The regional climate hindcast simulations were driven by data from the ERA-Interim reanalysis (Dee et al. 2011), which had been produced by the European Centre for Medium-Range Weather Forecasts (ECMWF). Data are available from 1979 to present with a horizontal grid spacing of 0.5° for eight times a day (00, 03, 06, 09, 12, 15, 18, and 21 UTC) with analyses at 00, 06, 12, and 18 UTC and forecasts at intermediate times.

Two 5-year periods have been simulated with CCLM (Table 1): the first period (1979–1983) covers the beginning of the ERA-Interim data set, while the second period ranges from 2008 to 2012. We have chosen the two most distant time periods to best grasp the rapid and consecutive warming in the region since 1997 (Dagvadorj et al. 2014). In this experimental design, which is of course not appropriate for evaluating a linear climate trend, we define trend in the following as the absolute difference between the second and first time periods.

Fig. 2 Orography (in meters a.s.l.) of the model domain on a latitude/longitude grid including locations of the used observing stations. *Stars* indicate the two weather stations from the Institute of Meteorology and Hydrology (IMH) in the region (Baitag in the south of the Altai, Duchinjil in the north in an Altai mountain valley), while *circles* locate the weather stations of the WATERCOPE project

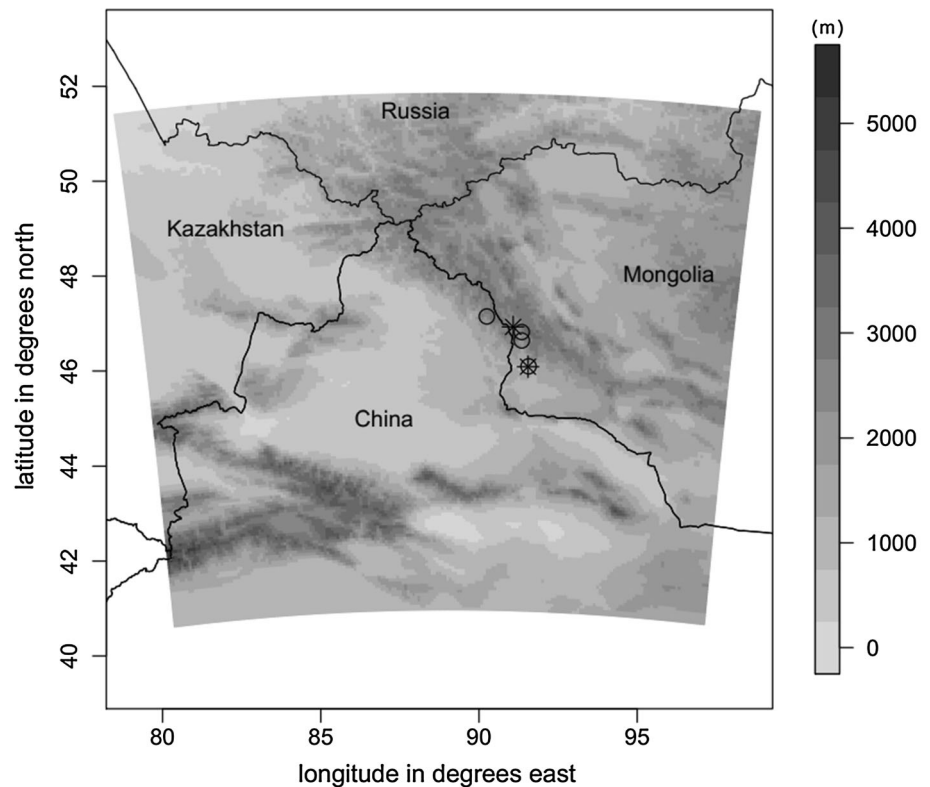


Table 1 Some properties of the 7 km resolution RCM and NWP simulations performed for this study for the model area, as depicted in Fig. 2

	CCLM (RCM)	COSMO (NWP)
Simulated period(s)	1979–1983 and 2008–2012	July 2013
Driving data	ERA-Interim	GME analysis
Simulation time step	60 s	40 s
Vertical atm. layers	40	60
Vertical soil layers	9	7
Output intervals	3 h	15 min

Regional weather forecast simulations were performed to evaluate the ability of COSMO to reproduce the vertical structure of the atmosphere. GME analyses were used as driving data for these simulations. GME was until recently the operational global circulation model of the German Meteorological Service (DWD) which features an icosahedral–hexagonal grid (Majewski et al. 2002), an equivalent grid spacing of approximately 20 km and 60 vertical layers. GME data are available every 3 h. Daily simulations were performed for July 2013, starting at 18 UTC (1 am local time).

For both types of simulation, a two time-level Runge–Kutta time-split scheme was used for the numerical integration with a time step of 60 s for the climate runs and 40 s for the weather runs. The setup includes a Kessler-

type (Kessler 1969) microphysics scheme handling cloud water, rain, snow, and cloud ice, a multilayer soil model (Schrodin and Heise 2002; Grasselt et al. 2008) with 9 and 7 layers, 40 and 60 atmospheric layers, a radiation scheme according to Ritter and Geleyn (1992), and the Tiedtke mass-flux convection scheme for moist convection (Tiedtke 1989) in the climate and weather simulations, respectively. Spectral nudging was not applied, as free model runs were investigated, so the model was supposed to develop its own dynamics.

3 Observational data

3.1 Climate stations

Observational data with high spatio-temporal resolution are lacking in the study region, especially in the high altitudes of the Altai. Therefore, our evaluations of the CCLM simulations concentrate on the operational climate stations as listed in Table 2. Data of two Mongolian climate stations operated by the Institute of Meteorology and Hydrology (IMH) of Mongolia (data displayed in Fig. 1) and four rain gauges (HOBO RG3-M) installed by the WATERCOPE project (see <http://www.watercope.org> for details on the project under which the experiment and the simulations were performed) are considered (for the station

Table 2 IMH (Baitag) and WATERCOPE climate/weather stations used for the climate hindcast evaluations

Station name	Country	Lat (°N)/lon (°E)	Station altitude (m)	Matching box surface altitude (m)	Appropriate box surface altitude (m)
Baitag*	MGL	46.09/91.55	1186	1242	Matching box
Duchinjil*	MGL	46.93/91.08	1951	2528	2312
Bulgan Soum	MGL	46.0988/91.5668	1181	1172	Matching box
Heltgii Had	MGL	46.6430/91.3527	1611	2207	2053
Turgen	MGL	46.8217/91.3500	1889	2412	2089
Aerqiate	CN	47.1503/90.2477	2121	2689	2358

The second column shows the country codes for Mongolia (MGL) and China (CN). Column five shows the ground level of the respective grid box in CCLM, which includes the location of the weather station (matching box). The ground altitude of the neighbouring grid box closest in height to the actual station ground level (appropriate box) is shown in column six

locations, see Fig. 2). Daily means or sums of 2-m (screen level) temperature and surface precipitation, respectively, measured at the IMH stations are used for the CCLM comparisons. The instantaneous precipitation observations from the WATERCOPE rain gauge stations are used for the short-term analysis for July 2013 in Sect. 4.4. The altitude of all utilised climate and weather stations varies between 1181 and 2121 m.

The orography around the two IMH stations Baitag and Duchinjil is fundamentally different. While Baitag is located in an extensive flat area at the foot of the Altai mountains bordering the Gobi desert, Duchinjil is located in a valley in the southern Altai mountains about 765 m higher and surrounded by high and steep mountains, which partly exceed 4000 m. At most of the considered weather stations, the ground altitude of the model grid box geographically containing the station differs from the station altitude by several hundreds of meters due to resolution effects. Thus, the ground altitude of neighbouring grid boxes, which are closer to the station altitude, are often used for the comparison with CCLM results (see Table 2) and lead to results closer to the observations in all cases.

3.2 Radio soundings

During field measurements in July 2013, 16 radiosondes were launched in the catchment of the Mongolian Bulgan River, which originates in the central Sino-Mongolian Altai and flows first to the south and turns the west when it enters the Gobi desert. The radiosondes (GRAW DFM-09) were launched at different times of the day at various locations across the area. Table 3 summarizes the soundings by location, time and altitude at launch time and specifies the COSMO forecast times used for comparisons. As the simulations were started at 01:00 local time, the day-ahead forecast was used for comparison with the 04:00 and 04:30 soundings to avoid a comparison during the model spin-up phase.

4 Results

In this section, we present the results of the dynamical downscaling of the ERA-Interim reanalysis with CCLM to highlight the potential added information. Then, both the reanalysis and the downscaling are compared with climate station observations to quantify the added value of the downscaling. Finally, weather simulations (COSMO) for July 2013 are compared with radio soundings to evaluate the ability of COSMO in reproducing the vertical thermodynamic structure of the atmosphere in this region.

When comparing CCLM downscaling with the driving ERA-Interim output, we are facing a change of support problem (Gotway Crawford and Young 2005), since the difference between the grid spacings of both data sets is relatively large (about 56 vs. 7 km). Although a comparison of CCLM and ERA-Interim output with point measurements is dominated by a change of support problem, the benefit and added values of CCLM become obvious this way from the climate data user perspective. The spatial coverage of observations is sparse in the study region, and a direct comparison with single weather stations is a reasonable method for a first evaluation of such high-resolution CCLM simulations.

4.1 Downscaling results

We first present example results for summer (JJA) and winter (DJF) from the dynamical downscaling of ERA-Interim for the periods 1979–1983 and 2008–2002, including trends (Fig. 3) to demonstrate its potential value as driving fields, e.g., for hydrological simulations and projections.

At first glance, the seasonal fields of 2-m temperature and precipitation amount from ERA-Interim and CCLM downscaling show very similar structures (left columns of Fig. 3a and b, respectively). As expected, the much more detailed topography impacting the CCLM simulations results in much more structured fields following roughly

Table 3 Radio soundings conducted in July 2013 with locations, launch times, geographical coordinates at launch times, start altitude, and model forecast times compared with (local time is UTC + 07)

Nr.	Start locations	Day/local times in July 2013	Start coordinates latitude (°N)/longitude (°E)	Start altitudes (m)	Compared model forecast times (h)
1	Bulgan Soum	09/05:00	46.0910/91.5484	1186	14
2	Bulgan Soum	10/04:30	46.0912/91.5485	1186	27.5
3	Bulgan Gol	11/19:00	46.3297/91.4308	1174	18
4	Yolt River	13/15:00	47.0912/91.1715	2248	14
5	near New Bulgan	14/14:30	47.1554/90.8487	2226	13.5
6	New Bulgan	15/11:00	46.9265/91.0931	1948	10
7	Shuvtir	16/11:30	46.7879/91.3085	1829	10.5
8	Summer Pasture	18/20:00	46.6449/91.5695	2393	19
9	Summer Pasture	19/04:30	46.6499/91.5841	2393	27.5
10	Summer Pasture	19/12:00	46.6598/91.5695	2416	11
11	Summer Pasture	19/19:30	46.6499/91.5695	2416	18.5
12	Summer Pasture	20/04:30	46.6415/91.5875	2393	27.5
13	Summer Pasture	24/04:00	46.6518/91.5888	2414	27
14	Turgen	24/14:00	46.8164/91.3512	1885	13
15	Bain Gol	24/20:00	46.8165/91.3513	1350	19
16	Bulgan Soum	26/14:00	46.0912/91.5483	1186	13

the topography. Accordingly, lower temperatures are found over the ridges and higher temperatures in the lowlands (left column in Fig. 3a). In general, CCLM produces, however, up to 5 °C higher 2-m temperatures over the flat lowlands, probably caused—at least in part—by the different land surface parameterizations employed for the reanalysis and in CCLM. Due to the much higher spatial resolution, the altitudes of the Altai range are much better resolved and extend much more to the south in the CCLM simulations than in ERA-Interim, leading overall to more precipitation by convection and orographic lift and an extension of the high precipitation fields further to the south. Visible is especially the increased winter precipitation over the south-western bounds of the Altai in CCLM, which is completely missing in the driving reanalysis. This detail is of importance for the regional agriculture, since it at least partly explains the higher abundance of water in Chinese Qinche catchment compared to the neighbouring Mongolian Bulgan catchment.

Partly even stronger differences are found for the different fields between the later period 2008–2012 and the earlier period 1979–1983. While ERA-Interim suggests increases in summer 2-m temperature over the more flat areas between 1.5 and 2.5 °C with the largest values in the northeast, CCLM simulates a smaller increase between 0.5 and 1.5 °C with the largest increase in the southern (Gobi) region. For the winter season both ERA-Interim and CCLM, see a temperature decrease everywhere. This decrease is, however, more pronounced in the reanalysis with values up to 4 °C in the north-eastern flatlands, while CCLM simulates lower increases reaching only

sporadically down to 3 °C at both the north-eastern and south-western foothills of the Altai.

Even stronger dissimilarities between ERA-Interim and its CCLM downscaling are obtained for precipitation. While ERA-Interim shows a dipole pattern in summer with considerable decreases in the north-eastern half of the region and moderate increases in the south-western part, CCLM shows moderate increases almost everywhere and specifically over the south-eastern foothills of the Altai and decreases over the north-western foothills. Thus, while ERA-Interim spreads the influence of the Altai range over the whole (CCLM) model domain, CCLM confines these influences to much smaller areas in the vicinity of the Altai and the Tian Shan mountains. The tendencies in winter are quite similar in structure between both fields, except that CCLM simulates increases almost everywhere, while the driving reanalysis shows large areas in the south and the northeast with negligible differences between both periods.

4.2 Validation studies

In this sub-section, we will first analyse the realism of ERA-Interim and its CCLM downscaling including its added value by comparison with the observations introduced in Sect. 3.

4.2.1 Annual cycles, inter-annual variability, and trends

We start with an observation-based overview of the temporal variability of the climate in the study region throughout the year based on the climate diagrams in Fig. 4

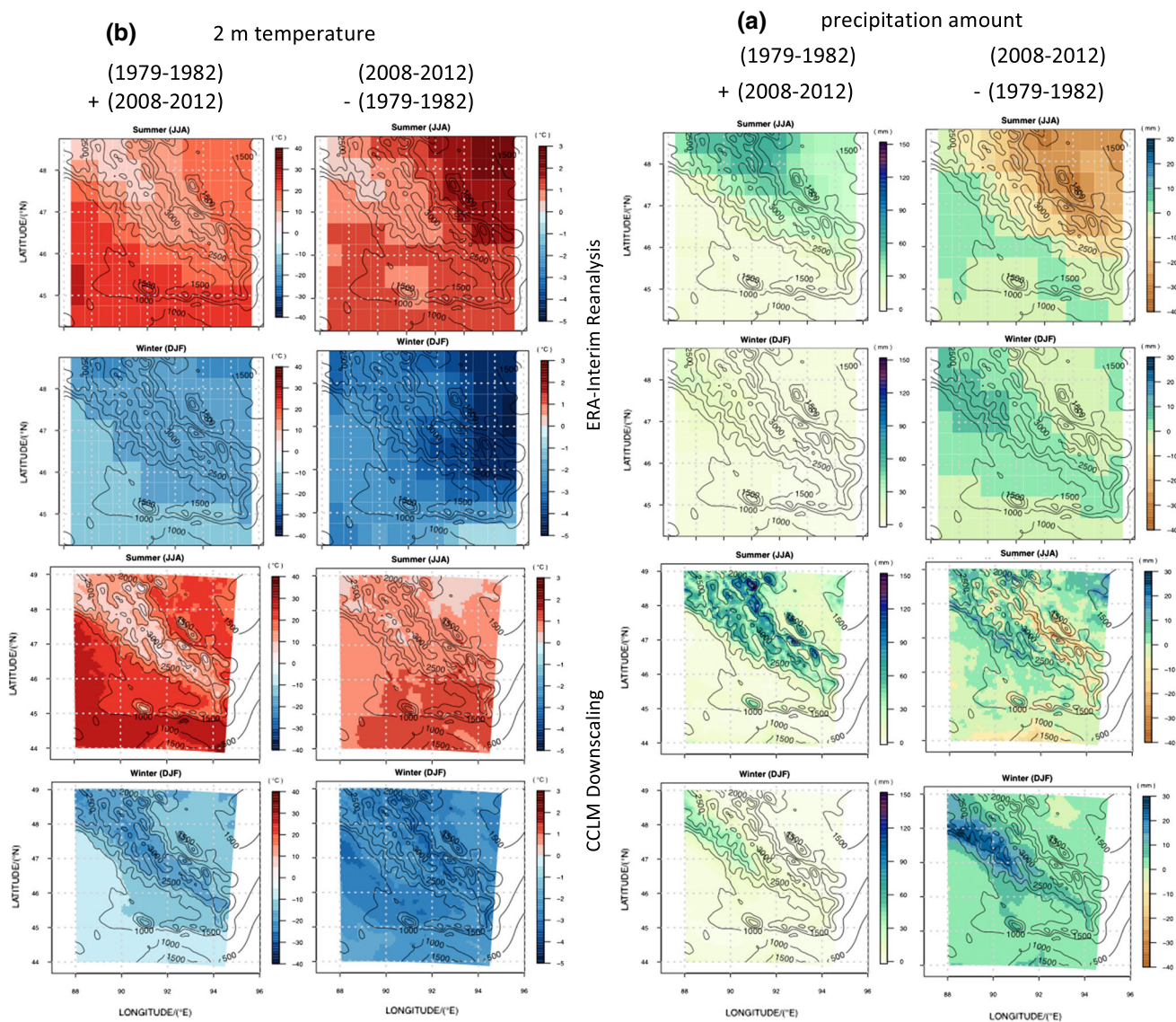


Fig. 3 Fields of seasonal mean (1979–1982 and 2008–2012) 2 m temperature and difference (2008–2012 minus 1979–1982) (a) and precipitation amounts (b) from ERA-Interim (upper half) and CCLM

downscaling (lower half) for summer (JJA) and winter (DJF) over the Sino-Mongolian Altai region as colour scale. The isolines show the topography as represented in the CCLM

for the periods 1979–1983 (left panels) and 2008–2012 (right panels) for the IMH stations Baitag (upper panels) and Duchinjl (lower panels). The diagrams also contain the respective values from ERA-Interim and the CCLM downscaling for the model grid areas containing the two stations. Figure 5 shows time series of seasonal precipitation sums and monthly mean temperatures, including the respective differences between observation and CCLM/ERA-Interim for both time periods in Baitag and Duchinjl.

For station Baitag bordering the Gobi desert, the CCLM simulations overestimate the monthly mean temperatures throughout the year (Figs. 4, 5) with the largest overestimations in winter by up to 9.6 °C (see February 2010). ERA-Interim, on the other hand, mostly underestimates

monthly mean temperatures (except for winter) by up to 5.3 °C during the months of March of the first period. During the latter period, also, the differences between ERA-Interim and CCLM are largest with up to 7.5 °C. Reanalysis and CCLM generally differ most markedly in winter and spring. Especially in the second period, CCLM simulations are closer to the observations in spring and autumn, while ERA-Interim is closer to the observations in winter. The largely parallel trends of the differences between ERA-Interim/CCLM and observation at Baitag (Fig. 5) suggest that CCLM-simulated temperatures are here highly influenced by the driving ERA-Interim data.

While the annual temperature curves are similar for both periods in Baitag, there are notable differences (Fig. 1).

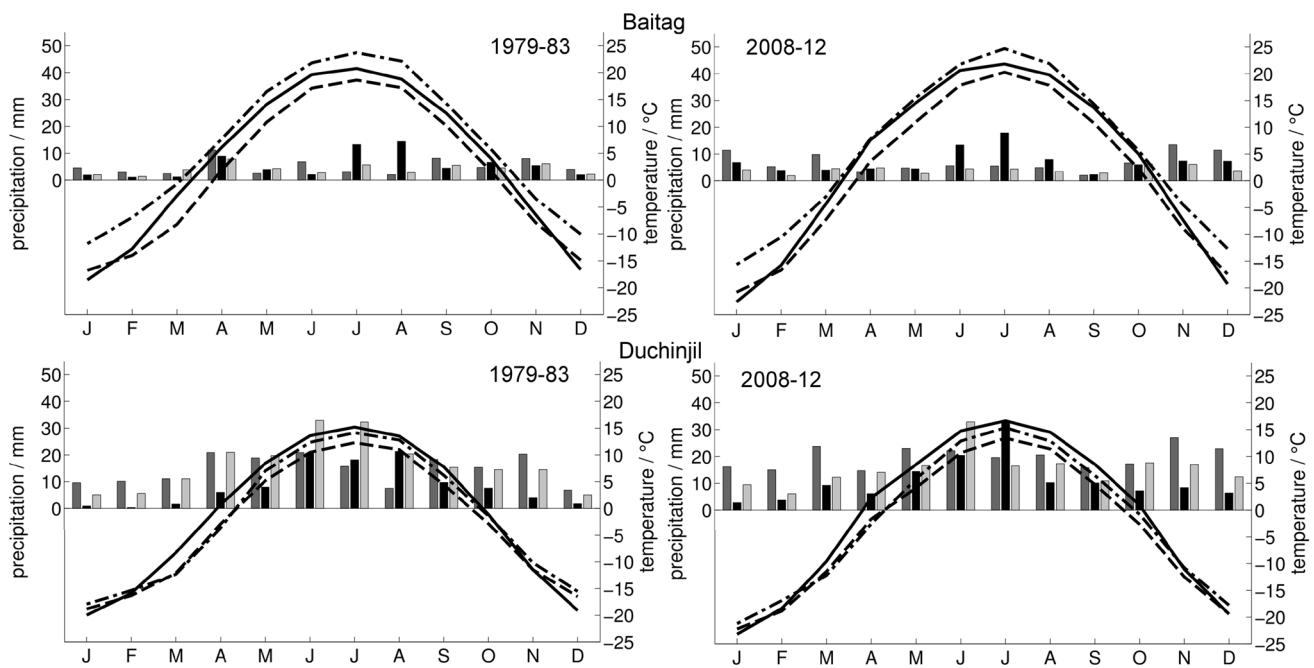


Fig. 4 Climate diagrams for two 5-year periods for station Baitag (upper panels) and station Duchinijil (lower panels). The left panels shows the period 1979–1983, the right panels the period 2008–2012. Bars indicate monthly mean precipitation (scales on the left axes)

with observations in black, CCLM simulations in dark grey, and ERA-Interim in light grey. The lines indicate monthly mean temperature (scales on the right axes) from observations (solid), CCLM (dotted-dashed), and ERA-Interim (dashed)

Summer temperatures have increased by 1–2 °C from the first to second periods. In contrast to the Mongolia-wide increase of winter temperatures (see Sect. 1), winter temperatures at Baitag were colder by about 4 °C in January during the second period compared to the first period, which underlines the peculiarity of the study region. These observed trends at Baitag are reproduced both by the ERA-Interim and by the CCLM-downscaled fields; the temperature decrease in winter is even more pronounced in the simulations.

The observed precipitation in Baitag reaches from less than 5 mm to above 60 mm per season with the highest values during the summer months. Both ERA-Interim and CCLM-downscaled fields do not reproduce this behaviour; especially for the second period both underestimate summer precipitation, and CCLM tends even to overestimate precipitation in winter. Over- and underestimations of precipitation by ERA-Interim are mostly passed on to the CCLM simulations (see difference plots in Fig. 5). The largest differences between ERA-Interim/CCLM and observation are found in summer (e.g., years 1983, 2010, and 2011).

According to the observations, total precipitation did increase by 32% from the first to second periods (Table 4) and maxima shifted from July/August to June/July. Contrary to ERA-Interim, the CCLM downscaling does reproduce the annual precipitation increase, while both model results do not reproduce the shift of the maxima

from summer to early summer. The precipitation increase by CCLM is, however, caused by an increased winter precipitation, which is not seen in the observations.

The seasonal cycles for Duchinijil (Fig. 5, lower panels) differ from Baitag due to the mountainous terrain and the higher altitude; while winter temperatures are similar at both stations, summer temperatures are significantly lower in Duchinijil. At both stations, the year-to-year variability of monthly mean temperatures in summer is smaller than in winter, which is also reproduced by ERA-Interim and CCLM downscaling (Fig. 5). Both reproduce better the Duchinijil temperature observations than the ones in Baitag with the largest differences in summer of up to 2.2 °C in the second period. Moreover, CCLM better follows the observed summer half-year observations than ERA-Interim, presumably due to the higher resolution and thus more accurate orography in CCLM. However, similar to Baitag, ERA-Interim slightly outperforms the CCLM downscaling in December and January. Differences between CCLM and ERA-Interim in Duchinijil are smallest in spring and largest in summer and autumn when CCLM is able to develop independent dynamics in the mountain area.

Some years (e.g., 2009 and 2011) show marked jumps in observed spring temperatures at both stations, which are probably related to the dissipation of the Siberian Anticyclone. The increasing frequency of cyclones approaching from westerly directions in spring can rapidly induce

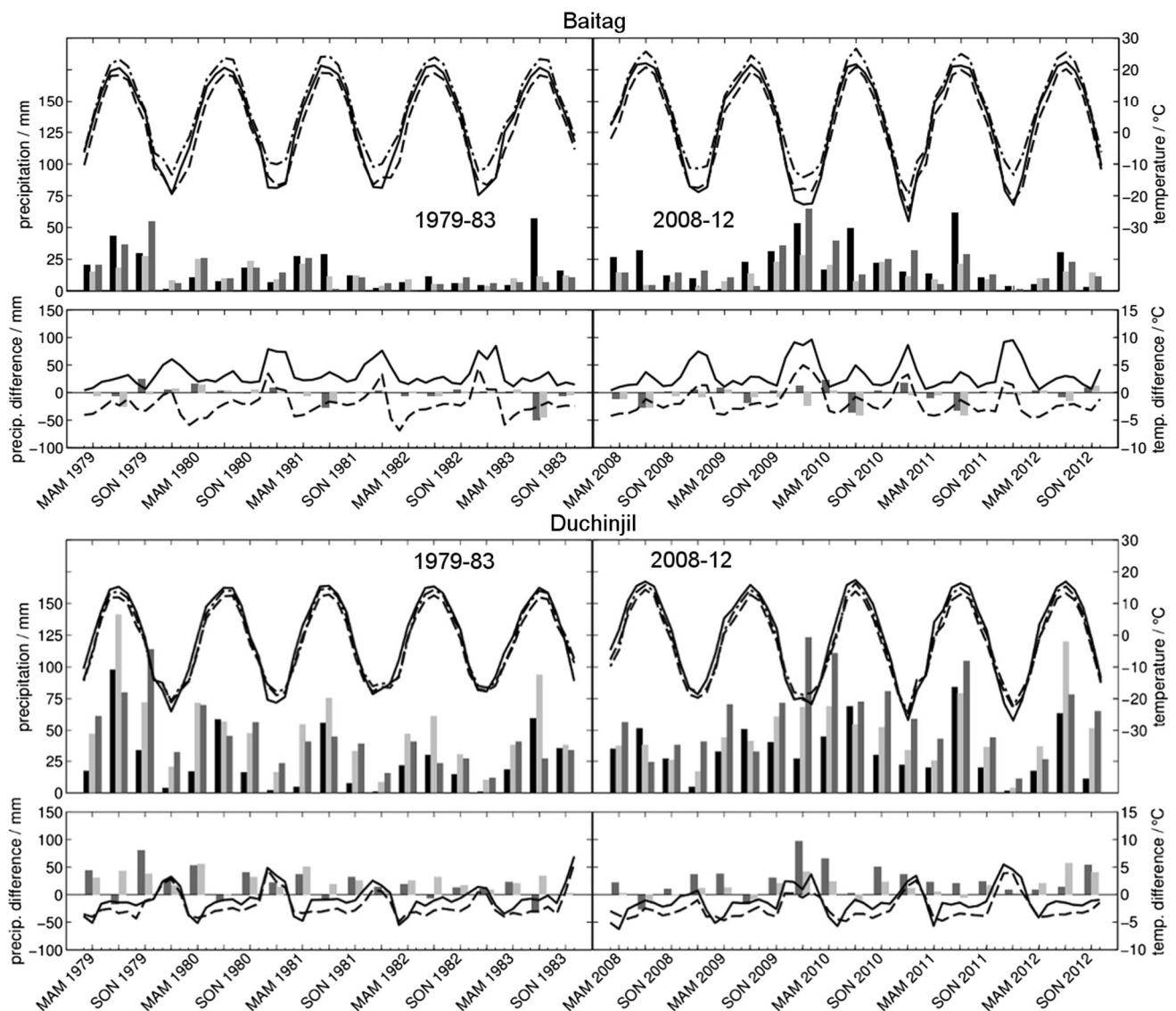


Fig. 5 Time series of seasonal precipitation (*bars*) and monthly mean 2 m temperature (*lines*) with differences between observations and the two model data for the stations Baitag (*upper half panels*) and Duchinjil (*lower half panels*). *Left panels* show the period 1979–1983, and *right panels* show the period 2008–2012. Precipitation is indicated by *black bars* for observations, *dark grey bars* for CCLM simulations, and *light grey bars* for ERA-Interim. Observed 2 m temperatures are shown as *solid lines* for observations, *dotted-dashed*

lines for CCLM simulations, and *dashed lines* for ERA-Interim. The differences between observation and ERA-Interim/CCLM are shown below the time series with CCLM precipitation minus observed precipitation as *dark grey bars*, ERA-Interim precipitation minus observed precipitation as *light grey bars*, CCLM 2 m temperature minus observed 2 m temperature as *solid lines*, and ERA-Interim 2 m temperature minus observed 2 m temperature as *dashed lines*

Table 4 Mean annual precipitation sums in mm from observations, ERA-Interim, and CCLM simulations for the two 5-year periods and the two climate stations

	Observations	ERA-Interim	CCLM
Baitag 1979–1983	65	49	60
Baitag 2008–2012	86	49	76
Duchinjil 1979–1983	100	198	176
Duchinjil 2008–2012	132	183	237

warmer temperatures (Bezuglova et al. 2012). Thus, the pronounced spring temperature underestimation by CCLM and ERA-Interim may be related to failures to reproduce these transitions.

At Duchinjil, the summer precipitation maximum is more prominent than at Baitag, and thus most probably related to enhanced summertime convection triggered by the mountains. Convective clouds are much more frequently found over the Altai mountains in summer compared to Baitag. Observed precipitation sums at both

locations are highly variable from season to season with maximum amounts of up to 100 mm in summer. ERA-Interim does reproduce the distinct summer maximum at Duchinjlil, which is less pronounced in the CCLM fields. Both simulations almost always overestimate summer precipitation, which is most pronounced in ERA-Interim (e.g., summer 1979 and 1983), while the opposite occurs in winter and spring.

4.2.2 Daily mean temperatures and precipitation sums

We now turn to the reproduction of observed daily temperature and precipitation statistics, i.e., the weather, by ERA-Interim and the CCLM-downscaled fields. Table 5 compares observed and CCLM-downscaled daily mean temperatures at Baitag bordering the Gobi desert and Duchinjlil within the Altai. The annual cycle in the data has been removed using spline regression (Wood 2006) to concentrate on the day-to-day variations (Simon et al. 2014). In Baitag correlations around 0.8 for summer, autumn and winter indicate a weaker relationship between CCLM and observations than during spring for which the correlation coefficient is 0.9. This pattern is also true for the relation of ERA-Interim with the observations, where

the highest correlation coefficient can be found for spring (0.8) and the lowest for winter (0.6). The large overestimation of winter temperature at Baitag by CCLM (Fig. 4) becomes also obvious in Table 5. The bias is at a moderate level in ERA-Interim. For Duchinjlil, we see a similar picture: the correlation coefficients between model output and observations are higher in spring and summer and drop during autumn and winter. However, CCLM outperforms ERA-Interim at both locations and in all seasons with respect to reproducing variability.

Precipitation amounts are very low in the study area (Table 4), and days above 10 mm are rare at both stations for all seasons (Fig. 6). The largest/lowest number of days above 5 mm are found in summer/winter, while in winter, not one single winter day above 10 mm was registered in Baitag within 10 years, and only one in Duchinjlil. At both stations, spring and autumn show similar observed distributions; only at Baitag autumn has somewhat more days with precipitation in all classes. At both stations, the relatively high frequencies for the more intense classes in summer stick out.

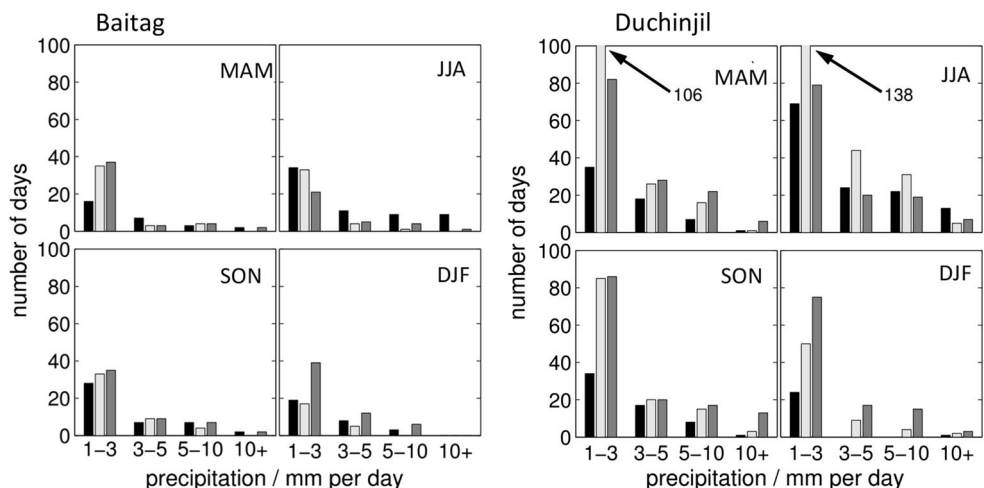
These overall tendencies are also reproduced by ERA-Interim and the CCLM-downscaled values, however, with different degrees of accuracy. For spring and autumn,

Table 5 Statistical measures for the comparison of daily mean 2 m temperatures between CCLM and observations, as shown in Fig. 5

	Baitag				Duchinjlil			
	ERA-Interim		CCLM		ERA-Interim		CCLM	
	CORR	BIAS	CORR	BIAS	CORR	BIAS	CORR	BIAS
Spring	0.83	-1.2	0.92	+1.9	0.77	0.71	0.82	-3.5
Summer	0.79	-0.3	0.84	+3.1	0.77	0.94	0.86	-1.2
Autumn	0.74	-1.4	0.81	+2.2	0.57	0.10	0.63	-0.7
Winter	0.63	1.7	0.79	+6.5	0.57	1.90	0.60	1.6

CORR is Pearson’s correlation coefficient and BIAS the bias in °C

Fig. 6 Histograms of daily precipitation sums for four intervals (1–3, 3–5, 5–10, and >10 mm/day) at stations Baitag (left) and Duchinjlil (right) for the years 1979–1983 and 2008–2012 (i.e., 10 years in total) for spring (MAM), summer (JJA), autumn (SON), and winter (DJF). Observations are indicated by black columns, CCLM by dark grey columns, and ERA-Interim by light grey columns



ERA-Interim and CCLM reproduce daily precipitation frequencies at Baitag to a similar degree, while the number of days with 5–10 mm/day and above is better reproduced by CCLM in all seasons and constitutes an added value of the downscaling concerning daily precipitation extremes. Daily precipitation below 3 mm is, however, mostly better reproduced by ERA-Interim. At the mountain station Duchinjl, both ERA-Interim and CCLM downscaling overestimate for spring and fall—but especially for winter—the number of precipitation days for all classes. In summer, both simulations generally reproduce the frequency distribution at Duchinjl with CCLM clearly outperforming ERA-Interim. Overall, however, CCLM generates the lowest inter-seasonal variation (see also Sect. 4.2.1).

4.2.3 Short-term precipitation extremes

We now turn to the analysis of precipitation at sub-daily intervals, which we analyse based on measurements from four WATERCOPE climate stations deployed in the valley of the Bulgan River at Bulgan Soum, Heltgii Had, Turgen, and Aerqiate in the Mongolian part of the region (Fig. 2; Table 2). The stations are located at different altitudes ranging from roughly 1000 to 2500 m a.s.l. Since these rain gauges were not heated and due to the short-time period for which measurements were available, we have to restrict the comparison to the summer months of 2012. Since ERA-Interim is available only at 3 hourly intervals, we further restrict our analysis to precipitation amounts during the same interval. The observations (black bars in Fig. 7) show increasing amounts of precipitation with increasing altitude in all intervals, as already observed for daily and monthly precipitation for the two IMH stations Baitag (close to Bulgan Sum) and Duchinjl (most close to Turgen), see also Sects. 4.2.1 and 4.2.2.

Except for the highest station Aerqiate, ERA-Interim largely overestimates the occurrence of events with 0.1–1 mm/3 h and largely underestimates the more intense

events, a well-known effect caused by the low spatial resolution of the reanalysis which has to represent a much larger area than the area of influence of a single station. Actually, ERA-Interim does not produce a single event with more than 3 mm/3 h. At Aerqiate, the number of low-intensity precipitation is—together with all precipitation classes—strongly underestimated by ERA-Interim, most probably because of the largely reduced topography in the model used for the reanalysis. Accordingly, also, the variability along the height gradient is strongly reduced in ERA-Interim compared to the observations. The CCLM downscaling significantly improves the frequency distributions, but with a tendency to overestimate with increasing altitude as already observed for the daily results. Overall, the downscaling considerably improves the results of the envisioned watershed-scale hydrological modelling. However, this analysis was performed for summer only. Snow cameras were installed at the WATERCOPE climate stations to better estimate winter precipitation also for larger areas. When their analysis becomes available, we will extend this analysis also to winter times, when from the results of Sect. 4.2.1 CCLM tends to overestimate precipitation.

4.2.4 Vertical structure of the troposphere

In this section, we evaluate the ability of the COSMO model to reproduce the vertical structure of the troposphere in the study area. To this goal, 16 radio soundings have been performed during a field experiments in July 2013 (see Sect. 3.2). Different from the CCLM downscaling of ERA-Interim, we now evaluate the ability of the (very similar) weather forecast version COSMO (see Sect. 2). Instead of ERA-Interim, we use the results of the global forecast model of DWD at the lateral boundaries of the regional model, similar to the study by Shrestha et al. (2015), who applied the same model quite successfully for the simulation of an extreme convective event over the Himalaya foothill region.

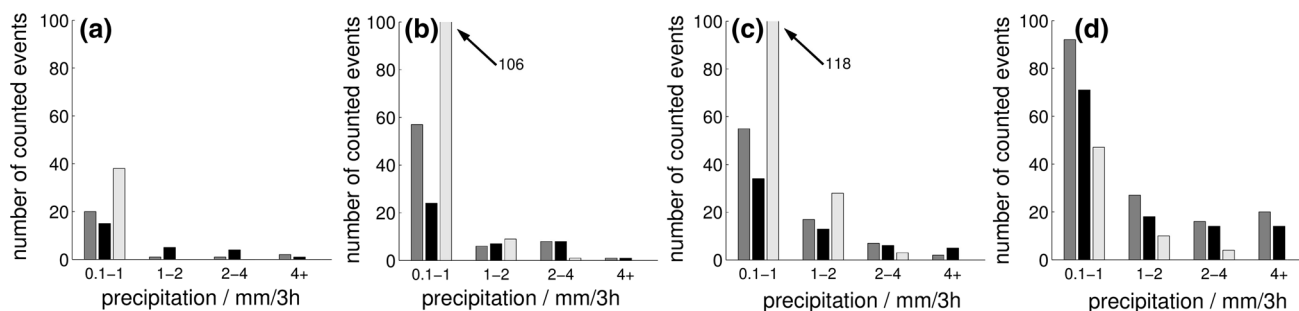


Fig. 7 Number of precipitation events for four intervals (0.1–1/3, 1–2/3, 2–4/3, and >4 mm/3 h) during summer 2012 for the WATERCOPE stations, **a** Bulgan Soum, **b** Heltgii Had, **c** Turgen,

and **d** Aerqiate. Observations are indicated by *black* columns, CCLM results by *dark grey* columns, and ERA-Interim results by *light grey* columns

Figure 8 compares ten vertical profiles of temperature and dew point simulated by COSMO with profiles observed by the radiosondes (Table 3). Not all 16 soundings are shown, since the remaining profiles do not provide extra information. The horizontal drift of the radiosondes during ascent (more than 100 km in some cases) was accounted for by choosing appropriate model boxes, which were selected according to drifts computed from the observed wind profile. The grey lines in Fig. 8 indicate model results for the nine grid box columns closest to the radiosonde start location. Their spread accounts for internal model variability and thus allows for a more objective comparison with the radiosonde ascents. While modelled

temperature profiles show relatively low variability (only up to 2 °C), it amounts to up to 10 °C for the dew point in the middle of the troposphere due to the more complex processes influencing humidity here. For the temperature, the largest horizontal variations occur in the lowest model layers due to the different surface altitudes of the neighbouring boxes.

Figure 8 displays the profiles only up to about 12 km height, which covers the troposphere in all cases. For the interpretation, we have to acknowledge differences of several hundred meters between the radiosonde starting altitudes and the lowest model layer due to the steep and complex terrain in the area. Except for the soundings 8 and

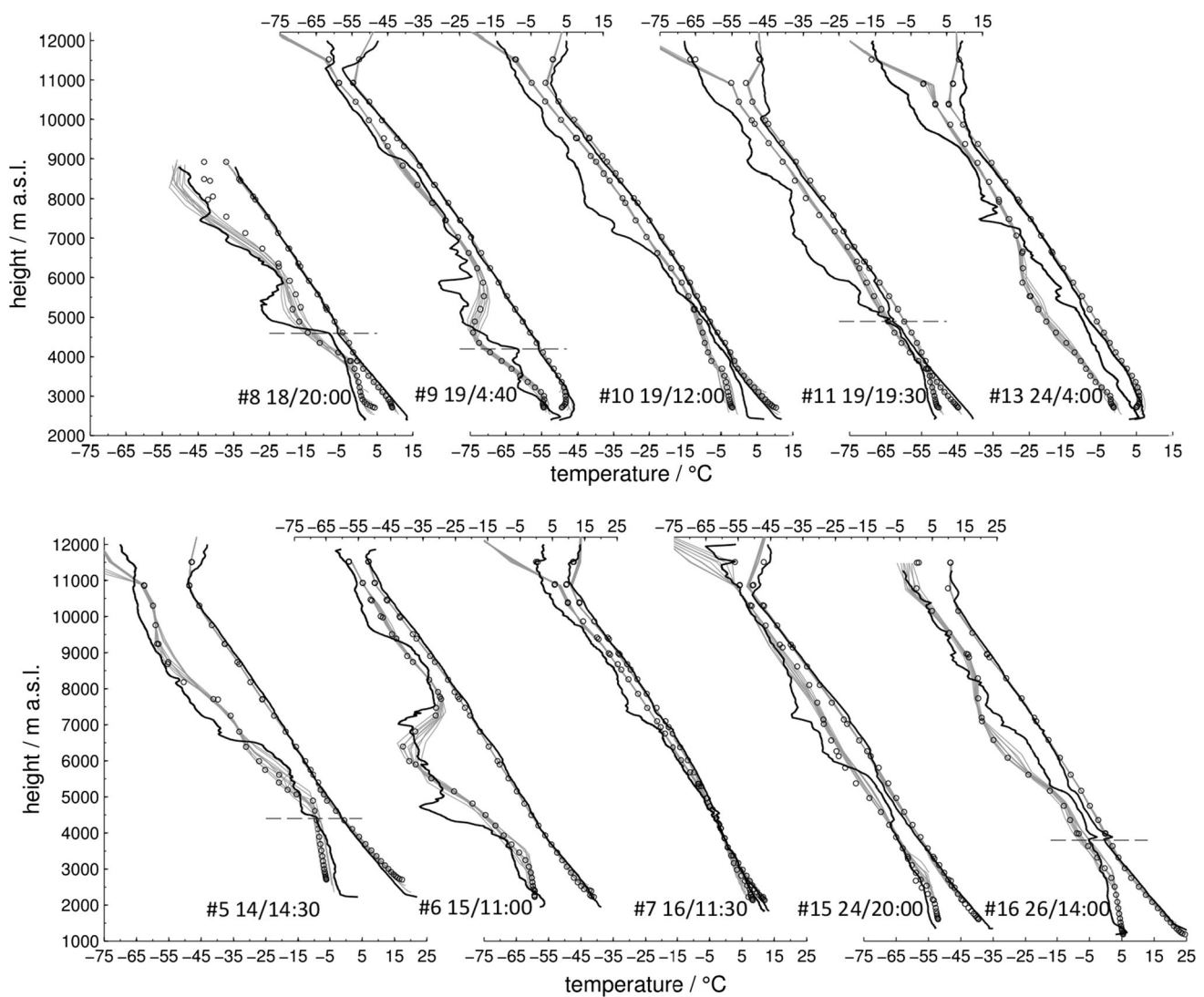


Fig. 8 Ten radio soundings indicated by number (*hash*), day in July 2013/local time according to Table 3. Five soundings are shown with the respective temperature axis either at the bottom (soundings 8, 10, and 13) or at the top (9 and 11). The *left-hand side* of each sounding shows the dew point and the *right hand side* the temperature. The

black lines denote the observations, the *open circles* show the COSMO values at grid level, the *grey lines* show the model profiles of the nine *grid box* columns surrounding the start location of the respective sonde, and the *horizontal dashed black lines* denote the assumed top height of the boundary layer if detectable

15, the drift adjustments, which amounted to a few degrees, were within the uncertainty range of the neighbouring columns.

When comparing model and observed profiles, we have to take into account the strong level-to-level fluctuations of the observed profiles, especially in the mid troposphere, which cannot be reproduced by a model due its limited vertical resolution. The height of the tropopause in the observations varied between 10 and 12 km and has been (except for sounding 11) captured very well by COSMO. The model is also very well able to reproduce observed profiles with dry conditions (e.g., profile 6) or very moist conditions (e.g., profile 7). Accordingly, a wide range exists both in the observations and the model. Obviously, COSMO shows both distinct dew point over- (e.g., profile 11) and underestimations (e.g., profile 13).

All soundings in the top row of Fig. 8 started at approximately the same location, i.e., a summer pasture close to lake Tsunkul' Nur, but at different times of the day and at different days. The lake has a diameter of approximately 2 km and is located in a structured valley roughly 7 km in diameter with surrounding ridges up to 200–500 m above the lake surface. Soundings 8, 9, and 10 show the development and decay of a night time near-ground inversion ending with a near-surface over-adiabatic stratification. This evolution is well captured by the model, but can only be judged qualitatively due to the height difference of the surface between radiosonde and model and its inability to recover the local topography well.

The correct reproduction of the atmospheric boundary layer (ABL), in particular its height, is indicative of a models ability to simulate the interaction of the atmosphere with the surface. Various definitions of the ABL and methods to estimate its height do exist (e.g., McGrath-Spangler and Denning 2013; Seidel et al. 2010), one indication being a capped temperature inversion (Kalthoff et al. 1998). Its determination from radio soundings in the study region is not straightforward. Only soundings 11 and 16 exhibit a marked capping inversion at about 4900 and 3800 m a.s.l., respectively, and in sounding 5 (4400 m), 8 (4600 m), and 9 (4200 m), a dew point recession accompanied by vertically constant temperature probably indicates the top of the ABL. The other soundings lack unambiguous signs of the ABL top, except the typical near-surface night time inversions visible and already discussed for soundings 8 and 9. In flat terrain typical ABL heights are between 1 and 2 km, while the observed ones are mostly between 2 and 3 km above ground, which is typical for mountainous terrain (e.g., Kossmann et al. 1998). Ma et al. (2011) observed PBL heights exceeding 4 km in May 2000 close to the Tibetan Plateau over Dunhuang in China, which is located about 800 km to the southwest of the study region.

In COSMO, the ABL height is difficult to detect via capping inversions because of the low vertical model resolution. While there are methods to obtain ABL heights from COSMO (Szintai et al. 2010; Szintai and Kaufmann 2008), but a detailed comparison between individual

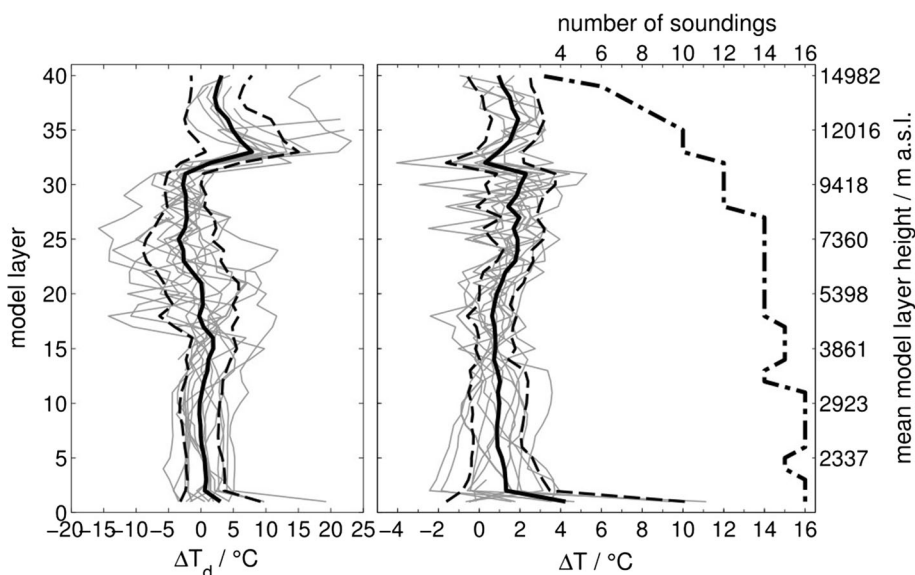


Fig. 9 Dew point difference (*left*) and temperature difference (*right*) between observations (radio sounding) and COSMO simulations for July 2013. The vertical axis is given by the model layer numbers shown on the *left*; the related mean model layer height is denoted on the *right*. The nearest neighbour values are chosen as the respective sounding data points. For all soundings of Table 3, the solid grey

lines show the difference between sonde and model. The mean difference is indicated by the solid black line, while the dashed lines denote the standard deviation. The number of soundings available for the calculation of mean and standard deviation is shown by the dashed-dotted line

observed and simulated ABL heights is not subject of this study. The differences between observations and model derived for all soundings in Table 3 are summarized in Fig. 9. Some (thin grey) lines exhibit gaps, because the correction for radiosonde drifts of the radiosondes may lead to height gaps when moving to another grid box column. Large mean temperature differences of up to 4 °C occur at the lowest model layer most probably due to the height differences between model and radiosonde at the ground. In the lower and middle tropospheres, the mean difference is about 1 °C which is within the measuring uncertainty. In the upper troposphere, the mean difference reaches 2 °C. On average, COSMO tends to overestimate the tropospheric temperature profile by 1–2 °C. Mean differences between modelled and observed dew point temperatures reach up to 8 °C in the height region of the tropopause and lower stratosphere, but large differences also occur again at the first model layer. The mean dew point is overestimated in the lower and middle tropospheres by up to 1.8 °C except for the first model layer, while in the upper troposphere, the dew point temperature is underestimated by up to 3.4 °C.

5 Discussion

In their WRF simulations, Sato and Xue (2013) found that the dynamical downscaling ability with regard to precipitation over Mongolia depends on the targeting year: e.g., major improvements of simulated summer precipitation were found in normal and the most wet years. Our study shows that dynamical downscaling overall improves especially summer precipitation when amounts are highest. Different from the findings of Sato and Xue (2013), our results (see Fig. 5; Table 4) do not suggest improved precipitation amounts in the wettest years; rather, the opposite is the case, and the strong inter-seasonal qualitative variability of simulated precipitation is more crucial. Our results in particular show (see Fig. 5) that both ERA-Interim and its downscaling by the CCLM do not reproduce the exceptionally cold 'zud' winters of 2010/11 and 2011/12.

Both observed and simulated precipitation amounts increase with altitude, although somewhat exaggerated by the model results. This demonstrates that CCLM adds spatial detail thanks to its more detailed orography compared to ERA-Interim. We assume that this leads to an improved representation of atmospheric flow and precipitation distribution in the Altai. However, CCLM produces too much precipitation, especially in spring, autumn, and winter. This seems to be a general problem with the COSMO model also over Europe, as pointed out, e.g., by Lindau and Simmer (2013). Many studies on dynamical

downscaling in Asia also found that the largest precipitation biases occur at mountain ridges (Rockel and Geyer 2008; Sato et al. 2007; Wang et al. 2013). Thus, future efforts should concentrate on the causes and remedies for this issue.

In their model, intercomparison for Asia Fu et al. (2005) found that the applied convection parameterisation scheme causes large differences in the regional climate simulation results. Rockel and Geyer (2008) likewise emphasise the importance of the convection scheme when considering model setup modifications. Furthermore, Klehmet et al. (2013) chose to reduce the minimal heat diffusion coefficient in their CCLM simulation over Siberia to reduce atmospheric mixing and obtain more realistic winter temperatures. Hence, a sensitivity study on the CCLM convection scheme and its tuning parameters should be performed for the study region.

Sato and Xue (2013) also point out that the WRF downscaling ability in their domain, which includes our study area, is sensitive to changes in the land surface parameterisation and that different initial soil moisture conditions did improve simulated precipitation amounts in dry years. Our study shows that CCLM produces too much precipitation during winter, while during summer, precipitation amounts were more realistic. In winter, the ground is frozen in the region, thus we assume that changes in the land surface parameterisation in the CCLM would not lead to improvements of simulated precipitation amounts. This conclusion is sided by results of Sato et al. (2007), who could not reduce their precipitation overestimates, when reducing the initial soil moisture in their NCEP driven TERC-RAMS simulation over Mongolia.

This study is not meant as a comprehensive assessment of climate change in the Altai region, but only a first step towards this aim. To fully investigate the influence of climate change on environmental conditions in the region, an ensemble approach to climate simulations following different scenarios and with different dynamical cores and physical parameterizations would be required (Schoelzel and Hense 2011). Such an approach would quantify the amplitude of uncertainty associated with the simulations and encompass natural climate variability.

6 Conclusions

We applied the limited-area model COSMO in its forecast and its regional climate model configuration (CCLM) for dynamical downscaling over the Altai region at very high resolution. The ERA-Interim reanalysis was downscaled with CCLM for two 5-year periods (1979–1983 and 2008–2012) to investigate its added value with respect to precipitation and 2 m temperature. Observations of two

weather stations maintained by the Institute of Meteorology and Hydrology (IMH) of Mongolia and four precipitation gauges installed by the WATERCOPE project have been used for comparison with the model output. We examined climate hindcasts of daily precipitation sums and mean 2 m temperature, including extremes, as well as sub-daily precipitation sums and extremes. Global analyses of DWDs global weather forecast model GME were dynamically downscaled to study the ability of the weather forecast version COSMO, which is practically identical to CCLM, to represent the vertical structure of the troposphere in the study region during a field experiment when 16 radio soundings were conducted in July 2013.

ERA-Interim underestimates 2 m temperature at the foothill station by up to 2 °C, except in winter, while the CCLM downscaling leads to a similar overestimate—except in spring and fall—but a strong overestimation by 5 °C in winter. This overestimation seems to be related to a shortcoming of CCLM to simulate strong inversions in the low atmosphere in this region. At the mountain station, the benefits of the dynamical downscaling become more visible. Here, the downscaled monthly mean 2 m temperatures are generally closer to the observations especially during the summer half-year compared to ERA-Interim.

Monthly precipitation sums in the region are usually much lower than 100 mm and have a pronounced maximum in summer. Monthly precipitation sums from ERA-Interim and its CCLM downscaling do not differ much in the flat area of Baitag, where they both fail to adequately reproduce the observed summer maximum. For the mountain station, both ERA-Interim and its CCLM downscaling overestimate monthly precipitation sums. ERA-Interim succeeds better in reproducing the relative summer precipitation maximum, while CCLM generally produces too much precipitation in winter but leads to improved summer precipitation sums. The largest differences between ERA-Interim and CCLM occur in summer with too much precipitation. In summary, the overall benefit of the dynamical downscaling regarding the annual cycle and inter-annual variability is small.

CCLM improves, however, clearly the frequency distributions of daily precipitation in the flat area of Baitag at all seasons and in summer also at the mountain station, where precipitation sums are largest. However, both ERA-Interim and CCLM produce too much daily precipitation in the mountains, and CCLM shows less realistic inter-seasonal differences in daily precipitation distributions. More distinct benefits of the dynamical downscaling become apparent on a three-hourly time-scale, where CCLM clearly improves the frequency distribution of precipitation sums, including its dependency on station altitude. Thus, the downscaling provides a clear added value for

hydrological simulations, which rely on good representations of the height dependency of precipitation.

The comparison of observed and simulated vertical profiles of temperature and dew point shows that the COSMO model is generally capable of simulating the vertical structure of the troposphere in the Altai in summer. Qualitatively, the model manages to simulate the height of the tropopause and near-ground effects, such as night time inversions and over-adiabatic stratification in summer. Temperature and dew point are most accurately simulated in the lower troposphere. Here, mean differences between observed and simulated temperature and dew point are between 1 and 2 °C, but increase with height. Thus, COSMO is able to produce realistically the tropospheric structure in summer in the Altai region. The quality of the downscaling might be improved by fine tuning the configuration of CCLM, especially for winter, but requires radio soundings, which are hard to get in this region.

Acknowledgements We would like to thank the WATERCOPE project for the funding of Oyunmunkh Byambaa, the provision of their climate station data, and for setting up and financing the field experiment in 2013. WATERCOPE was funded by the International Fund for Agricultural Development (IFAD) under Grant I-R-1284. We also thank the Institute of Meteorology and Hydrology (IMH) of Mongolia for providing us with the station measurements.

Open Access This article is distributed under the terms of the Creative Commons Attribution 4.0 International License (<http://creativecommons.org/licenses/by/4.0/>), which permits unrestricted use, distribution, and reproduction in any medium, provided you give appropriate credit to the original author(s) and the source, provide a link to the Creative Commons license, and indicate if changes were made.

References

- Arakawa A, Lamb VR (1977) Computational design of the basic dynamical processes in the UCLA general circulation model. *Methods Comput Phys* 17:173–265
- Bachner S, Kapala A, Simmer C (2008) Evaluation of precipitation characteristics in the CLM and their sensitivity to parameterizations. *Meteorol Z* 17:407–420. doi:10.1127/0941-2948/2008/0300
- Bastola S, Misra V (2014) Evaluation of dynamically downscaled reanalysis precipitation data for hydrological application. *Hydrol Process* 28:1989–2002
- Batima P (2006) Climate change vulnerability and adaptation in the livestock sector of Mongolia. Assessments of Impacts and Adaptations to Climate Change (AIACC) Project Office
- Batima P, Natsagdorj L, Gomboluudev P, Erdenetsetseg B (2005) Observed climate change in Mongolia. Assessments of Impacts and Adaptations to Climate Change (AIACC) Project
- Batima P, Bold B, Sainkhuu T, Bavuu M (2008) Adapting to Drought, Zud and Climate Change in Mongolia's Rangelands. In: Leary N, Conde C, Kulkarni J, Nyong A, Pulhin J (eds) Climate change and vulnerability. The International START Secretariat
- Bezuglova NN, Zinchenko GS, Malygina NS, Papina TS, Barlyayeva TV (2012) Response of high-mountain Altai thermal regime to

- climate global warming of recent decades. *Theor Appl Climatol* 110:595–605
- Boehm U, Kuecken M, Ahrens W, Block A, Hauffe D, Keuler K, Rockel B, Will A (2006) CLM: the climate version of Im: brief description and long-term applications. *COSMO Newsletter* 6
- Chen F, Yuan YJ, Wei WS, Fan ZA, Zhang TW, Shang HM, Zhang RB, Yu SL, Ji CR, Li Qin (2012) Climate response of ring width and maximum latewood density of *Larix sibirica* in the Altay mountain reveals recent warming trend. *Ann Forest Sci*. doi:10.1007/s13595-012-0187-2
- Chen F, Yuan YJ, Wei WS, Zhang TW (2014) Precipitation reconstruction for the southern Altay Mountains (China) from tree rings of Siberian spruce, reveals recent wetting trend. *Dendrochronologia* 32:266–272
- Chotamonsak C, Salathé EP, Kreasuwan J, Chantara S, Siri-witayakorn K (2011) Projected climate change over Southeast Asia simulated using a WRF regional climate model. *Atmos Sci Lett* 12:213–219
- Dagvadorj D, Natsagdorj L, Dorjpurev J, Namkhainyam B (2010) Mongolia assessment report on climate change 2009. Ministry of Environment, Nature and Tourism. ISBN 978-99929-934-3-X
- Dagvadorj D, Batjargal Z, Natsagdorj L (2014) Mongolia second assessment report on climate change-2014, Ministry of Environment and Green Development of Mongolia
- Dairaku K, Emori S, Nozawa T (2008) Impacts of Global Warming on Hydrological Cycles in the Asian Monsoon Region. *Adv Atmos Sci* 25:960–973
- Davi NK, Jacoby GC, D'Arrigo RD, Baatarbileg N, Curtis AE (2009) Tree-ring-based drought index reconstruction for far-western Mongolia: 1565–2004. *Int J Climatol* 29:1508–1514. doi:10.1002/joc.1798
- Davi NK, D'Arrigo RD, Jacoby GC, Cook ER, Anchukaitis KJ, Nachin B, Rao MP, Leland C (2015) A long-term context (931–2005 C.E.) for rapid warming over Central Asia. *Quatern Sci Rev* 121:89–97
- Dee DP, Uppala SM, Simmons AJ, Berrisford P, Poli P, Kobayashi S, Andrae U, Balmaseda MA, Balsamo G, Bauer P, Bechtold P, Beljaars ACM, van de Berg L, Bidlot J, Bormann N, Delsol C, Dragani R, Fuentes M, Geer AJ, Haimberger L, Healy SB, Hersbach H, Hólm EV, Isaksen I, Kållberg P, Köhler M, Matricardi M, McNally AP, Monge-Sanz BM, Morcrette JJ, Park BK, Peubey C, de Rosnay P, Tavolato C, Thépaut JN, Vitart F (2011) The ERA-Interim reanalysis: configuration and performance of the data assimilation system. *Q J R Meteorol Soc* 137:553–597
- Dobler A, Ahrens B (2008) Precipitation by a regional climate model and bias correction in Europe and South Asia. *Meteorol Z* 17:499–509
- Dobler A, Ahrens B (2010) Analysis of the Indian summer monsoon system in the regional climate model COSMO-CLM. *J Geophys Res* 115:D16101
- Doms G (2011) A description of the nonhydrostatic regional COSMO Model, Part I: Dynamics and Numerics. Deutscher Wetterdienst, Offenbach
- Doms G, Foerstner J, Heise E, Herzog HJ, Mironov D, Raschendorfer M, Reinhardt T, Ritter B, Schrodin R, Schulz JP, Vogel G (2011) A description of the Nonhydrostatic Regional COSMO Model—Part II: Physical Parameterization. Deutscher Wetterdienst, Offenbach
- Dulamsuren C, Khishigjargal M, Leuschner C, Hauck M (2014) Response of tree-ring width to climate warming and selective logging in larch forests of the Mongolian Altai. *J Plant Ecol* 7:24–38
- Flint L, Flint AL (2012) Downscaling future climate scenarios to fine scales for hydrologic and ecological modeling and analysis. *Ecological Process*. doi:10.1186/2192-1709-1-2
- Fowler HJ, Blenkinsop S, Tebaldi C (2007) Linking climate change modelling to impacts studies: recent advances in downscaling techniques for hydrological modelling. *Int J Climatol* 27:1547–1578
- Fu CB, Wang SY, Xiong Z, Gutowski WJ, Lee DK, McGregor JL, Sato Y, Kato H, Kim JW, Suh MS (2005) Regional climate model intercomparison project for Asia. *Bull Am Meteorol Soc* 86:257–266
- Gao XI, Shi Y, Giorgi F (2011) A high resolution simulation of climate change over China. *Sci China Earth Sci* 54:462–472
- Giorgi F, Christensen J, Hulme M, von Storch H, Whetton P, Jones R, Mearns L, Fu C, Arritt R, Bates B, Benestad R, Boer G, Buishand A, Castro M, Chen D, Cramer W, Crane R, Crossly J, Dehn M, Dethloff K, Dippner J, Emori S, Francisco R, Fyfe J, Gerstengarbe F, Gutowski W, Gyalistras D, Hanssen-Bauer I, Hantel M, Hassell D, Heimann D, Jack C, Jacobeit J, Kato H, Katz R, Kauker F, Knutson T, Lal M, Landsea C, Laprise R, Leung L, Lynch A, May W, McGregor J, Miller N, Murphy J, Ribalaygua J, Rinke A, Rummukainen M, Semazzi F, Walsh K, Werner P, Widmann M, Wilby R, Wild M, Xue Y (2001) Regional climate information—evaluation and projections, climate change 2001: the scientific basis. In: Houghton JT et al. (eds) *Contribution of Working Group to the Third Assessment Report of the Intergovernmental Panel on Climate Change*. Cambridge University Press, Cambridge
- Giorgi F, Jones C, Asrar GR (2009) Addressing climate information needs at the regional level: the CORDEX framework. *WMO Bulletin* 58:175–183
- Gomboluudev P (2012) Climate change of Mongolia. Integrated water management national assessment report: Volume I. DDC 555.7/015i-57
- Gotway Crawford CA, Young LJ (2005) Change of support: an interdisciplinary challenge. In: Renard P, Demougeot-Renard H, Froidevaux R (eds) *Proc. of the Fifth European Conference on Geostatistics for Environmental Applications, geoENV V*, Neuchatel, Switzerland. Springer, Berlin
- Grasselt R, Schuettemeyer D, Warrach-Sagi K, Ament F, Simmer C (2008) Validation of TERRA-ML with discharge measurements. *Meteorol Z* 17(6):763–773
- Kalthoff N, Binder HJ, Kossmann M, Vögtlin R, Corsmeier U, Fiedler F, Schlager H (1998) Temporal evolution and spatial variation of the boundary layer over complex terrain. *Atmos Environ* 32:1179–1194
- Kamp U, McManigal KG, Dashtseren A, Walther M (2013) Documenting glacial changes between 1910, 1970, 1992 and 2010 in the Turgen Mountains, Mongolian Altai, using repeat photographs, topographic maps, and satellite imagery. *Geogr J* 179:248–263
- Kessler E (1969) On the distribution and continuity of water substance in atmospheric circulations. *Meteor Monogr* 10(32):1–84
- Kim J, Jung HS, Mechoso CR, Kang HS (2008) Validation of a multidecadal RCM hindcast over East Asia. *Glob Planet Chang* 61:225–241
- Klehmet K, Geyer B, Rockel B (2013) A regional climate model hindcast for Siberia: analysis of snow water equivalent. *The Cryosphere* 7:1017–1034
- Kossmann M, Voegtlin R, Corsmeier U, Vogel B, Fiedler F, Binder HJ, Kalthoff N, Beyrich F (1998) Aspects of the convective boundary layer structure over complex terrain. *Atmos Environ* 32:1323–1348
- Leung LR, Ghan SJ, Zhao ZC, Luo Y, Wang WC, Wei HL (1999) Intercomparison of regional climate simulations of the 1991 summer monsoon in eastern Asia. *J Geophys Res* 104:6425–6454

- Leung LR, Mearns LO, Giorgi F, Wilby RL (2003) Regional climate research: needs and opportunities. *Bull Am Meteorol Soc* 84:89–95
- Lindau R, Simmer C (2013) On correcting precipitation as simulated by the regional climate model COSMO-CLM with daily rain gauge observations. *Meteorol Atmos Phys* 119(1–2):31–42. doi:10.1007/s00703-012-0215-7
- Liu S, Gao W, Liang XZ (2013) A regional climate model downscaling projection of China future climate change. *Clim Dyn* 41:1871–1884
- Ma M, Pu Z, Wang S, Zhang Q (2011) Characteristics and numerical simulations of extremely large atmospheric boundary-layer heights over an arid region in north–west China. *Boundary-Layer Meteorol* 140:163–176
- Majewski D, Liermann D, Prohl P, Ritter B, Buchhold M, Hanisch T, Paul G, Wergen W, Baumgardner J (2002) The operational global icosahedral-hexagonal gridpoint model GME: description and high-resolution tests. *Mon Weather Rev* 130:319–338
- Mannig B, Mueller M, Starke E, Merckenschlager C, Mao W, Zhi X, Podzun R, Jacob D, Paeth H (2013) Dynamical downscaling of climate change in Central Asia. *Glob Planet Chang* 110:26–39
- Maussion F, Scherer D, Mölg T, Collier E, Curio J, Finkelnburg R (2014) Precipitation seasonality and variability over the Tibetan Plateau as resolved by the High Asia Reanalysis. *J Climate* 27:1910–1927
- McGrath-Spangler EL, Denning AS (2013) Global seasonal variations of midday planetary boundary layer depth from CALIPSO space-borne LIDAR. *J Geophys Res.* doi:10.1002/jgrd.50198
- Murphy J (1999) An evaluation of statistical and dynamical techniques for downscaling local climate. *J Clim* 12:2256–2284
- Ozturk T, Altinsoy H, Turkes M, Kurnaz ML (2012) Simulation of temperature and precipitation climatology for the Central Asia CORDEX domain using RegCM 4.0. *Clim Res* 52:63–76
- Pederson N, Jacoby GC, D'Arrigo RD, Cook ER, Buckley BM, Dugarjav C, Mijiddorj (2000) Hydrometeorological reconstructions for northeastern Mongolia derived from tree rings: 1651–1995. *J Climate* 14:872–881
- Qian Y, Leung LR, Ghan SJ, Giorgi F (2003) Regional climate effects of aerosols over China: modeling and observation. *Tellus B* 55:914–934
- Ritter B, Geleyn JF (1992) A comprehensive radiation scheme for numerical weather prediction models with potential applications in climate simulations. *Mon Weather Rev* 120:303–325
- Rockel B, Geyer B (2008) The performance of the regional climate model CLM in different climate regions, based on the example of precipitation. *Meteorol Z* 17:487–498
- Rockel B, Will A, Hense A (2008) The regional climate model COSMO-CLM (CCLM). *Meteorol Z* 17:347–348
- Rummukainen M (2010) State-of-the-art with regional climate models. *WIREs. Clim Change* 1:82–96
- Sato T, Xue Y (2013) Validating a regional climate model's downscaling ability for East Asian summer monsoonal interannual variability. *Clim Dyn* 41:2411–2426
- Sato T, Kimura F, Kitoh A (2007) Projection of global warming onto regional precipitation over Mongolia using a regional climate model. *J Hydrol* 333:144–154
- Schiemann R, Luethi D, Vidale PL, Schaer C (2008) The precipitation climate of Central Asia: intercomparison of observational and numerical data sources in a remote semiarid region. *Int J Climatol* 28:295–314
- Schluetz F, Lehmkuhl F (2007) Climatic change in the Russian Altai, southern Siberia, based on palynological and geomorphological results, with implications for climatic teleconnections and human history since the middle Holocene. *Veg Hist Archaeobot* 16:101–118
- Schoelzel C, Hense A (2011) Probabilistic assessment of regional climate change in Southwest Germany by ensemble dressing. *Clim Dyn* 36:2003–2014
- Schrodin E, Heise E (2002) A new multi-layer soil model. *COSOM Newsletter* 2
- Schwikowski M, Eichler A, Kalugin I, Ovtchinnikov D, Papina T (2009) Past climate variability in the Altai. *PAGES News* 17:44–45
- Seidel DJ, Ao CO, Li K (2010) Estimating climatological planetary boundary layer heights from radiosonde observations: comparison of methods and uncertainty analysis. *J Geophys Res.* doi:10.1029/2009JD013680
- Shrestha P, Dimri AP, Schomburg A, Simmer C (2015) Improved understanding of an extreme rainfall event at the Himalayan Foothills: a case study using COSMO. *Tellus A* 67:26031. doi:10.3402/tellusa.v67.26031
- Simon T, Wang D, Hense A, Simmer C, Ohlwein C (2014) Generation and transfer of internal variability in a regional climate model. *Tellus A.* doi:10.3402/tellusa.v65i0.22485
- Siurua H, Swift J (2002) Drought and zud but no famine (Yet) in the mongolian herding economy. *IDS Bull* 33:88–97
- Szintai B, Kaufmann P (2008) TKE as a Measure of Turbulence. *COSMO Newsletter* 8
- Szintai B, Kaufmann P, Rotach MW (2010) Simulation of Pollutant Transport in Complex Terrain with a Numerical Weather Prediction-Particle Dispersion Model Combination. *Boundary-Layer Meteorol* 137(3):373–396
- Tiedtke M (1989) A comprehensive mass flux scheme for cumulus parameterization in large-scale models. *Mon Weather Rev* 117:1779–1800
- Viviroli D, Archer DR, Buytaert W, Fowler HJ, Greenwood GB, Hamlet AF, Huang Y, Koboltschnig G, Litaor MI, López-Moreno JJ, Lorentz S, Schaedler B, Schreier H, Schwaiger K, Vuille M, Woods R (2011) Climate change and mountain water resources: overview and recommendations for research, management and policy. *Hydrol Earth Syst Sci* 15:471–504
- Wang D, Menz C, Simon T, Simmer C, Ohlwein C (2013) Regional dynamical downscaling with CCLM over East Asia. *Meteorol Atmos Phys* 121:39–53
- Wood S (2006) Generalized additive models: an introduction with R. Chapman and Hall/CRC, Boca Raton
- Wood AW, Leung LR, Sridhar V, Lettenmaier DP (2004) Hydrologic implications of dynamical and statistical approaches to downscaling climate model outputs. *Clim Chang* 62:189–216
- WWF Mongolia Programme Office (2012) Buyant river basin modeling: results of hydraulic and hydrological modeling. WWF Report
- Yatagai A, Yasunari T (1994) Trends and decadal-scale fluctuations of surface air temperature and precipitation over china and mongolia during recent 40 year period (1951–1990). *J Meteorol Soc Jpn* 72–6:937–957
- Yin Y (2006) Vulnerability and Adaptation to Climate Variability and Change in Western China. Assessments of Impacts and Adaptations to Climate Change (AIACC) Project
- Zhang TW, Yuan YJ, Hu YC, Wei WS, Shang HM, Huang L, Zhang RB, Chen F, Yu SL, Fan ZA, Qin L (2015) Early summer temperature changes in the southern Altai Mountains of Central Asia during the past 300 years. *Quatern Int* 358:68–76